MDPI

Article

Human-robot cooperative adaptive reinforcement constraint control for a lower limb rehabilitation exoskeleton using user movement intention

Rafael Perez-San Lazaro [1,*], Rita Q. Fuentes Aguilar [2] and Isaac Chairez [2]

[1] Tecnológico de Monterrey, School of Engineering and Sciences, Zapopan, Jalisco Mexico; rafael.sanlazaro@tec.mx
[2] Tecnológico de Monterrey, Institute of Advanced Materials for Sustainable Manufacturing, Zapopan, Jalisco, Mexico; rita.fuentes@tec.mx, isaac.chairez@tec.mx
* Correspondence: rafael.sanlazaro@tec.mx

Abstract: Exoskeletons used for rehabilitation must operate together with the human user to adapt to the biomechanical-inspired movements of the regular human gait cycle rather than operate by following a predefined trajectory without considering the human-robot interaction effects. This work presents the assessment of a lower limb exoskeleton whose motion is performed according to a collaborative approach given the movements of the human user and the relative force concerning the exoskeleton structure. The OpenSim software generates both the forces and motions people exert during the gait cycle. These forces and movements are compared to the results of a virtual model that considers the interaction between the user and the exoskeleton in two possible interaction scenarios. The first one contemplates the implementation of a position controller to generate interaction-independent movement of the exoskeleton and the forces it exerts on the user. The second case considers the force exerted by the exoskeleton on the patient to trigger a force-based controller after trespassing a predefined exoskeleton hold, leading to a hybrid control scheme. Using this approach, the exoskeleton can actively collaborate with the user and provide motion only when required responding to a free motion if the user is not working in opposition to the exoskeleton motion. This novel strategy permits the evaluation of a hybrid position-force controller for wearing the active orthosis. Numeric simulations show the performance of the proposed system, comparing the results with those obtained from similar collaborative approaches. These outcomes confirm the supposed advantages of the proposed controller.

Keywords: Human-robot collaboration; hybrid systems; lower limb exoskeleton; force control; constraint control.

Citation: Lastname, F.; Lastname, F.; Lastname, F. Title. *Sensors* **2022**, *1*, 0.

Received:
Accepted:
Published:

1. Introduction

Lower limb exoskeletons are active anthropomorphic wearable robotic orthoses supporting the body. Depending on the rehabilitation task, the exoskeleton must enforce the controlled motion of articulations or align with the user's motion [1]. These devices can be categorized within the following main groups [2]:

- Augmentation exoskeletons are intended for healthy users and do not replace any ability nor help the user recover the lost capacities.
- Assistance exoskeletons are mainly used by patients who permanently lose the ability to walk and use these devices for their daily activities.
- Rehabilitation exoskeletons aimed to help patients regain mobility through repetitive training strategies.

For the mentioned exoskeleton categories, human-robot interaction is a key issue in the development of lower limb exoskeletons. However, its importance is greater regarding rehabilitation and assistance exoskeletons, as the interaction directly affects the outcome

of the rehabilitation therapy or the quality of the assistive process [3]. Even when several research directions consider the interaction between the exoskeleton and the user, it is possible to identify exoskeleton dominant areas, which include the introduction of novel design proposals, the integration of multiple sensor information, and the implementation of controlled gait generation that depends on the user's motion [4].

An assistive lower-limb exoskeleton comprises a controlled robotic system hanging the human lower limbs to increase the muscles' strength and articular motion accuracy of a healthy or impaired person's legs. Robotic manipulators are more effective at activities demanding strong forces and repetitive accuracy than humans are at complex scenario analysis and diagnosis. The finest of both operative conditions can be combined to create adaptive man-machine systems for power assistance, rehabilitation, teleoperation, and haptic engagement in virtual reality. Most of the created exoskeletons are designed to approach the first two groups with power. Only a few systems are being researched to carry out precise positioning activities to interact with the environment physically. The latter application needs complex control algorithms to plan and carry out leg motions along predetermined trajectories while identifying interaction forces of the exoskeleton with the user and environment.

XXXXXXXXXXXXXXX

XXXXXXXXXXXXXXX

The previous arguments on the potential operative scenarios open new research areas in user-machine interactive controls, psychological acceptance, and structurally integrated sensor systems. The primary objective is collaborating with robots rather than having humans take their place. Due to the tight interaction between the user and the robotic equipment, lower-limb exoskeletons pose a unique difficulty for this vision. When the robotic system performs a leg movement on a desired path, portable exoskeletons enable haptic support with intuitive guiding. The user proceeds down this route, modifying their movement to influence the action they are performing. Because of this, the user always takes the initiative while executing a task. Several assistive exoskeleton uses, including self-feeding for disabled people, orthopedic surgery, and positioning duties during daily activities, are made possible by this safety feature.

A hybrid motion/force controller is required in many automation activities where the robot interacts with the environment (or the user in the case of exoskeletons) and must be able to regulate both position and force. Exoskeleton robot controllers having a single control objective, such as force regulation or position control, have been the subject of in-depth research. Designing a position controller in a joint or task space is an option. Designing force controllers is more complicated because of how the environment interacts with it and how difficult it is to define the interaction model.

Force cannot be precisely regulated, but impedance and admittance controllers can create a mass-spring-damper model between the end-effector and the environment. Accurate force tracking can be accomplished by including force feedback in the position controller. Approaches without sensors have been devised when force sensors are inaccessible [8]. Although many position or force controllers are available, there are still few options for hybrid position/force controllers, and creating a reliable hybrid controller is still an active research topic. The motion and force controllers are applied in two complementary sub-spaces, leading to the stability analysis of each in one widely used position/force controller introduced in [5]. The controller is inheritable. The constraint is challenging to satisfy throughout the process (for instance, contact loss is possible), and the orthogonality depends on the choice of coordinate and metric [6,7]. Therefore the controller is not robust.

This study develops a hybrid position-force controller for regulating the motion of the joints of a lower-limb exoskeleton for rehabilitation purposes. This controller mobilizes the joints in a controlled manner if the norm of the generalized vector of forces has a value below a given exoskeleton defined by the practitioner. If this norm overpasses the expected exoskeleton, the force controller acts, tracking an expected reference differential force between the exoskeleton and the user. The hybrid control formulation includes a set

of adaptive gains that force the inclusion of joint constraints in the control design. This direct adaptive algorithm introduces a formal manner to regulate the motion to fulfill the effective tracking of reference trajectories and the reference forces and keep the motion of all joints inside the valid set considering the mechanical configuration of the exoskeleton.

The main contributions of this study are:

- The development of a hybrid position-force controller for a lower-limb exoskeleton implemented in a virtual environment. The controller considers the state restrictions for each joint in the leg structures.
- The development of a formal virtual system that relates the lower limb exoskeleton with a virtual user representation considering the force interaction between the components.
- The adaptive law that regulates the controller gains based on applying a particular controlled Lyapunov function. The gains are regulated using the tracking error as input information.

This manuscript is organized as follows: Section 2 describes the details of the virtual robotic exoskeleton and its interaction with the user considering the introduction of the force detector. Section 3 details the controller structure, the switching rule, and the manner that defines the transition between controllers. Section 4 details the implementation aspects of the proposed controller, including the application of the virtualized exoskeleton and the associated user. Section 5 reviews the simulated results corresponding to the application of the hybrid position-force controller using the information obtained from the virtualized system. Section 6 closes this study with some conclusions and some potential future trends.

2. Human-robot virtual setup

This paper considers implementing a virtual model that defines the interaction between a lower limb exoskeleton and a user. In this strategy, the exoskeleton is designed in Solidworks^{TM}, and the user is represented by a human model, which is a modified version from a design taken from *grabcad.com*, available at *https://grabcad.com/library/articulated-dummy-1*.

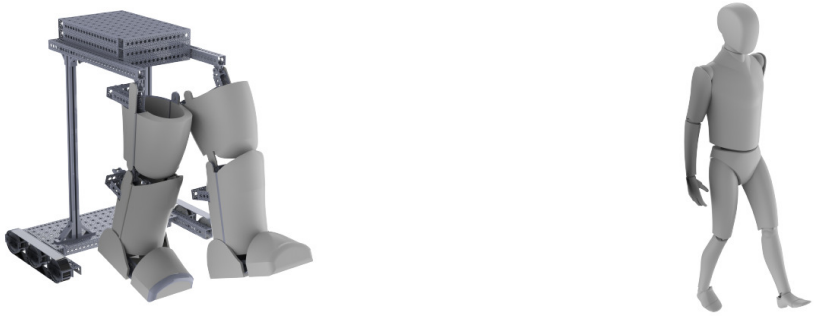

(a) Lower limb exoskeleton **(b)** Virtual human model

Figure 1. Elements of the virtualized exoskeleton-user system to evaluate the suggested position-force controller.

Figure 1 shows the complete lower limb exoskeleton (Figure 1a). The design of the exoskeleton device results from the development of a mobile device that includes three degrees of freedom in each leg to generate controlled motion in the hip, knee, and ankles in the sagittal plane. The combined structure uses the exoskeleton, and the user is presented with a caterpillar-like robot that provides the system with autonomous displacement. This work is explained in detail in [8], where the implementation of an adaptive sliding-mode controller for this device is presented. This figure also illustrates the virtual human model (Figure 1b) that defines the interaction force between the exoskeleton and the virtual user. The virtual human model is modified to allow the hip, knees, and ankles to move in the sagittal

plane, leaving the rest of the available joints as fixed structures. Both models are coupled so that the joints from the hip, knees, and ankles are aligned between the exoskeleton and the human model.

Figure 2. Human-exoskeleton virtual model considering the interaction components between structures.

Figure 2 presents how the two systems are coupled, simulating the exoskeleton's utilization with the proposed user. Notice how the complete system has several possible degrees of freedom. However, all the components remain fixed except those that allow the movement of the hip, knees, and ankles from both the exoskeleton and the user, leaving a total of 12 degrees of freedom: 6 for the exoskeleton and 6 for the user for the aforementioned joints per lower limb.

This study considers the utilization of data obtained from *Opensim*^{TM} [9] to characterize the forces obtained from the user. *Opensim*^{TM} is a software that enables musculoskeletal modeling and dynamic simulation of biomechanical processes for two main purposes. The first one comprehends the definition of the reference trajectories for each joint of interest throughout the complete human gait cycle, while the second one aims to define the force that is generated at each joint during the gait cycle.

Figure 3 shows the obtained reference trajectories for each one of the six target joints through the complete human gait cycle. These trajectories correspond to the selected model with its corresponding motion. Even when these results are presented in other works [10], this study considers the data from *Opensim* to relate all the biomechanical results to the same motion.

Figure 4 depicts the total fiber force exerted at each joint during the gait cycle. This force is computed by summing all (in terms of the norm of that vector) the individual forces from the muscles involved during the movement at each joint. The cases considered here apply to each lower extremity and correspond to the flexion and extension of the hip and to the bending and extension of the knees. The force exerted by the ankles is omitted for the simplicity of this study.

Opensim includes a set of different musculoskeletal models that enable analyzing different biomechanical aspects. This study considers utilizing the *Gait2392* model from those models. It is an exoskeleton-dimensional model with 23 degrees of freedom contemplating lower extremity joint definitions, low back joint of the proposed exoskeleton, and a planar knee model. It also features 92 muscle-tendon actuators representing 76 lower extremities and torso muscles. It is important to recall that this model represents an approximately 1.8 m tall subject with a mass of around 75.16 kg. Such anatomical measures corresponded to a

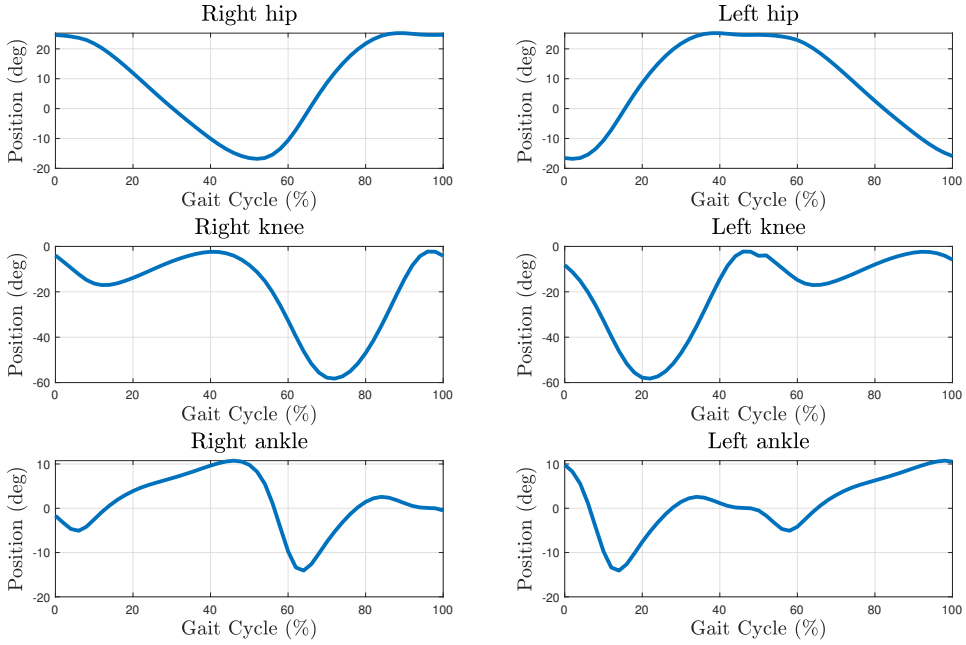

Figure 3. Reference trajectories for human gait

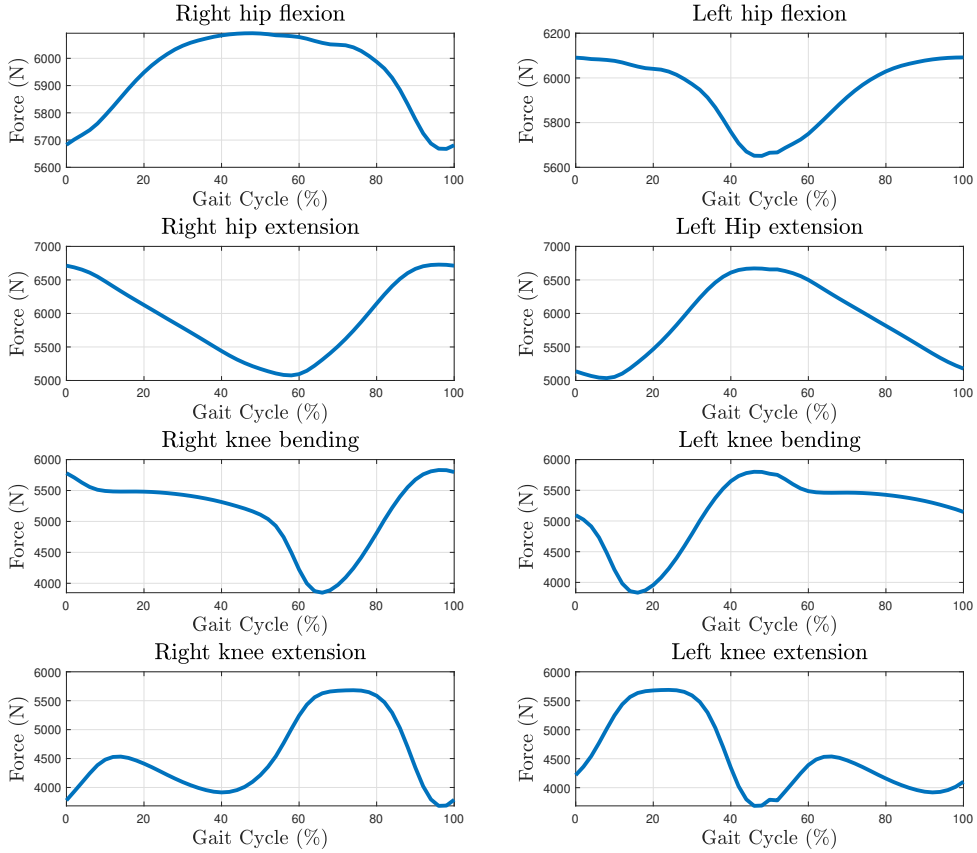

Figure 4. Total fiber force exerted during human gait

regular human configuration. This model can be loaded with different motions. However, for this study, the model integrates the motion for the human gait cycle in healthy patients

(*normal motion*). Figure 5 illustrates the model with the aforementioned represented muscles.

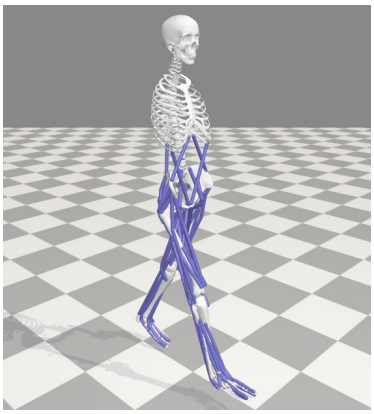

Figure 5. *Opensim Gait2392* model loaded with *normal motion*.

The model from *Opensim* has its reference frames, from which the angles from the lower limb joints are measured. Figure 6 illustrates the frames the model considers for hip, knee, and ankle joints. This model considers the clockwise direction negative angle values and the anti-clockwise direction positive. Considering these reference frames and directions is paramount for the simulation, as these characteristics must be aligned with the models from Solidworks^{TM}.

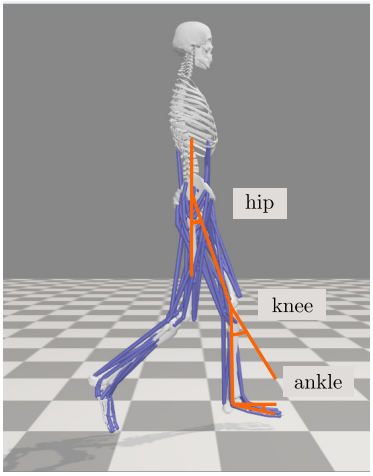

(a) Lower limb target joints

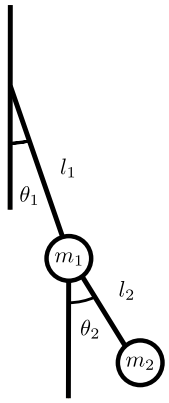

(b) Geometrical model

Figure 6. Lower limb diagrams

Figure 6a shows the exoskeleton joints considered for the design of the exoskeleton (hip, knee, and ankle). However, this work considers the implementation of the hybrid position-force controller only for the joints of the hip and the knee. Nonetheless, the proposed device enables the possibility of including the ankle joints for further studies. Taking into account that only the joints of the hip and knee are considered, each lower limb can be represented as a double pendulum system, as illustrated in figure 6b, where l_1 $[m]$ and l_2 $[m]$ are the lengths of the links of the system, m_1 $[kg]$; and m_2 $[kg]$ are the corresponding masses, and θ_1 $[deg]$ and θ_2 $[deg]$ are the angular positions that are formed at each joint. This simplified way of understanding the leg configuration permits to the construction of the nominal model of the exoskeleton device.

Table 1. Muscles considered for each motion

Motion	Muscles that are considered
Hip flexion	Adductor Brevis, Adductor Longus, Gluteus Medius 1, Gluteus Minimus 1, Gracilis, Iliacus, Pectineus, Psoas Major, Rectus Femoris, Sartorius, and Tensor Fasciae Latae
Hip extension	Adductor Longus, Adductor Magnus 1, Adductor Magnus 2, Biceps Femoris-Long Head, Gluteus Maximus 1, Gluteus Maximus 2, Gluteus Maximus 3, Gluteus Medius 3, Gluteus Minimus 3, Semimembranosus, Semitendinosus
Knee bending	Biceps Femoris-Long Head, Biceps Femoris-Short Head, Gracilis, Lateral Gastrocnemius, Medial Gastrocnemius, Sartorius, Semimembranosus, Semitendinosus
Knee extension	Rectus Femoris, Vastus Intermedius, Vastus Lateralis, Vastus Medialis

Table 1 shows the muscles considered for one of the four cases for this study. For all cases, the corresponding muscles are considered depending on whether the left or lower limb is studied.

2.1. Integration in the Simulink environment for position-force hybrid control

The obtained data from *Opensim*™ (Figures 3 and 4) serve as a reference for the proposed controller, which considers both the joints motion and the force that is generated throughout the gait cycle. These data are included within the Simulink™ environment. Similarly, the virtual model generated in Solidworks™ is exported to Simulink™ through the Simscape Multibody Link Plugin. Once the data from *Opensim* and the model from Solidworks™ are both in the Simulink™ environment, these elements are integrated for the analysis of the system.

In summary, there are two separate models: the first corresponds to the exoskeleton, whereas the second corresponds to the user's virtual representation. The approach used in this work consists of generating motion first in the robotic device and, according to the action it makes, a force is exerted on the virtual model of the user to generate its controlled motion. Furthermore, the force generated between the exoskeleton and the user is contemplated. This force is only measured in the sagittal plane, where a greater force is applied, considering that the motion in each joint is also in the same plane. This measurement is made by utilizing the *Spatial Contact Force* block from the Simscape™ Utilities section. This block makes a convex hull representation of the file from Solidworks™, so the pieces where the force between the user and the exoskeleton is measured have to be segmented to relate the spacial contact force block with specific areas of the piece, rather than the whole part. Figure 7 shows the piece segmentation corresponding to the left lower limb. Notice that it is segmented into 12 different pieces, and the ones highlighted in blue are the regions where the force is measured. The back region measures the force generated in the posterior region of the lower limb, while the front region measures the force located in the anterior region.

As a consequence, there are two force sensors per joint, one for the anterior region and the other for the posterior region. Leading to a total of 6 force sensors, considering the hip and knee joints for both lower limbs. However, these sensors are coupled in pairs to activate the force control per joint when the detected force trespasses the defined exoskeleton in both the anterior and posterior regions.

3. Human-robot hybrid position-force control

This section presents the fundamentals of hybrid systems required for the control design. In addition, the control design is presented considering the adaptive gains regulated using the constraints information. The explicit definitions of the position and force tracking controllers are also considered.

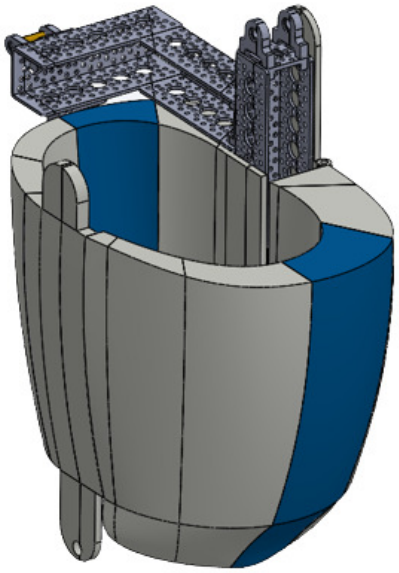

Figure 7. Lower limb target joints from the *Opensim* model, including the components that are represented as force sensors for the interaction with the user.

3.1. Preliminaries

There are four fundamental phases to the movement of the rehabilitation exoskeleton. Each is distinguished by discrete dynamic changes and continuous dynamical models (defined mainly by the event when the vector of forces between the device and the user goes above the referred exoskeleton). The mathematical model utilized to represent the back-and-forth of continuous and discrete dynamics results in a class of hybrid systems for the rehabilitation exoskeleton [11]. Suppose a typical mono-directional walking gait is utilized. In that case, the transitions between the continuous phases follow an orderly pattern even though a fixed periodicity does not determine the change from continuous to discrete dynamics and vice versa. This dynamical property serves as the driving force behind the application of the multi-domain hybrid systems architecture, which is based on a predetermined sequence of phases (or domains) forming a coherent cycle.

The mathematical model of a general multi-domain hybrid controller is characterized as the tuple [12] corresponding to $\mathcal{HD} = (\Gamma, D, U, S, \Delta, FG)$. Here $\Gamma = (V; E)$ is the sequenced cycle. Consequently, $v \in V$ defines a given set of vertexes for the subdomains, v^+ represents the subsequent vertex of v in the cycle of the gait cycle. In addition, $e = \{v \to v^+\}$ establishes the transition starting at the analyzed vertex v to v^+.

Holonomic constraints. In view of the exoskeleton model defined by the set of coordinates $q \in Q$. Here $Q \in \mathbb{R}^n$ defines the configuration space of the device with n degrees of freedom (DOF). The specific dynamics of the exoskeleton in a given domain depend on the Lagrangian of the model and the constraints for the individual states.

All physical contacts of the robot sections with the exoskeleton imply a holonomic constraint defined as $\eta_c(q)$. Assume that C_v is the indexing set of all holonomic constraints, characterized as D_v. We propose some holonomic constraints depending on the state evolving in the domain as $\eta_c(q) = \{\eta_c(q)\}_{c \in C_v}$. The associated kinematic constraints are given by $J_v(q)\dot{q} = 0$, where $J_v(q)$ is the Jacobian matrix of $\eta_c(q)$, i.e.,

$$J_v(q) = \frac{\partial \eta_c(q)}{\partial q}$$

Continuous Dynamics. Using the information of mass, inertia, and length properties for each link in the exoskeleton, The equation of motion in the proposed domain D_v is established using the Euler-Lagrange theory [13].

$$\begin{aligned} \dot{x}_a(t) &= x_b(t) \\ \dot{x}_b(t) &= f(x_a(t), x_b(t)) + g(x_a(t))u(t) + \\ & D^{-1}(x_a(t))J_v^{\top}(x_a(t))F_v(x_a(t), x_b(t)) + \xi(x_a(t), x_b(t), t) \end{aligned} \tag{1}$$

Here $x_a \in \mathbb{R}^n$, $x_b \in \mathbb{R}^n$ and $u \in \mathbb{R}^n$ are vectors defining the position, velocity, and control respectively. The vector function $f : \mathbb{R}^n \times \mathbb{R}^n \to \mathbb{R}^n$ is the drift term which could be estimated as $f(x_a, x_b) = -D^{-1}(x_a)[C(x_a, x_b)x_b + G(x_a)]$. The term $D : \mathbb{R}^n \to \mathbb{R}^{n\times n}$ defines the inertia matrix. The term $C : \mathbb{R}^n \times \mathbb{R}^n \to \mathbb{R}^{n\times n}$ defines the Coriolis matrix, The vector term $G : \mathbb{R}^n \to \mathbb{R}^n$ characterizes the gravitational components. The input matrix is $g : \mathbb{R}^n \to \mathbb{R}^{n\times n}$ characterizing the effect of the input signal on the state dynamics. This matrix is invertible, that $g = D^{-1}$. The vector function $\xi : \mathbb{R}^n \times \mathbb{R}^{n_v} \times \mathbb{R} \to \mathbb{R}^n$ defines the effect of external time-dependent perturbations and internal state-dependent uncertainties in the exoskeleton. The function $F_v : TQ \times U_v \to \mathbb{R}^{n_v}$ (with n_v the number of total holonomic restrictions) explicit the contact wrenches related to constraint forces and/or rotation moments. Here TQ is the set of active states when the contact wrenches activate, and U_v is the related controllers connected to the contact wrenches u_v. Intending to study the holonomic constraints, the second-order differentiation of the state-dependent constraints is going to be set to a null value, that is

$$J_v(x_a)\dot{x}_b + \dot{J}_v(x_a, x_b)x_b = 0 \tag{2}$$

The restricted systems dynamics are established using the expression of (1) and (2) simultaneously.

Domains and Guards. The amount of forces and moments generated by holonomic restrictions is constrained. We expressly state these requirements as inequalities $\nu_v F_v(q, \dot{q}, u_v) \geq 0$, where ν_v is a function containing the exoskeleton's parameters. Defining the acceptable configurations of the exoskeleton is completed by the so-called unilateral restrictions $h_v(x_a) \geq 0$ (specified in the set U_v). The domain of admissibility D_v, therefore takes the following form:

$$D_v = \{(q, \dot{q}, u_v) \in TQ \times U_v \mid \nu_v F_v(q, \dot{q}, u_v) \geq 0, \;\; h_v(x_a) \geq 0\} \tag{3}$$

Here $v \in V$, that defines the boundary of the domain subspace. The set called guard S_e is the proper subset of the edge of the admissible domain D_v, determined by the limit condition related to the transition from D_v to the subsequent domain, D_v^+. Here $H_e(x_a; x_b; u_v)$ is the appropriate component from the set D_v corresponding to the edge condition; then the guard is defined as

$$S_e = \left\{(x_a, x_b, u_v) \in TQ \times U_v \mid H_e(x_a, x_b, u_v) = 0; \quad \dot{H}_e(x_a, x_b, u_v) < 0\right\} \tag{4}$$

Discrete Dynamics.

A reset map R_e connected to the guard's system states S_e links the guard's system states to the following domain. Using a reset map R_e and the assumption of a smooth transition from the position to the force control-oriented domain [14], the states after the transition of $Dv+$ are computed given the pre-impact states $(x_a^-; x_b^-)$ on S_e. Following the discussion in [15], the configurations of the system are invariant across an impact, i.e., $(x - a; x + a)$, but post-impact velocities must meet the smooth transition equation:

$$\begin{bmatrix} D(x_a^-) & -J_{v^+}^\top(x_a^-) \\ J_{v^+}^\top(x_a^-) & 0 \end{bmatrix} \cdot \begin{bmatrix} x_b^+ \\ \delta F_v \end{bmatrix} = \begin{bmatrix} D(x_a^-)x_b^- \\ 0 \end{bmatrix} \tag{5}$$

where δ defines the impulse function for the forces in the exoskeleton during contact with the user.

Virtual Constraints. Like holonomic constraints, virtual constraints are a set of functions that regulate a robot's behavior to accomplish specifically intended trajectories (also known as the tracking errors in the control literature). The phrase *virtual* refers to the notion that feedback control is used to impose these limitations rather than physical ones.

XXXXXXXXXXXXX

XXXXXXXXXXXXX

Virtual constraints are the difference between the current and desired outputs from the exoskeleton, that is, $\Delta_{a,v} = x_{a,v} - x_{a,v}^d$ and $\Delta_{b,v} = x_{b,v} - x_{b,v}^d$ for $v \in V$, where $x_{a,v}$ and $x_{b,v}$ are the current position and velocity respectively. The time-dependent functions $x_{a,v}^d$ and $x_{b,v}^d$ are the desired trajectories that are twice differentiable. These desired trajectories are proposed accordingly to the technique proposed in [13]. This method established a technique to design monotonic and differentiable trajectories over a gait cycle [16,17]. This design is motivated by the proposed autonomous controller.

Notice that the design of the autonomous controller only needs to solve the steering of $\Delta_{a,v}$ and $\Delta_{b,v}$ to the origin within each continuous domain. Notice that it is unnecessary to drive the tracking errors to the invariant set defined by the origin through discrete dynamics. Indeed, this may be a complicated and even unfeasible solution because of the mechanical restrictions in the exoskeleton.

Considering that the BR should move over stepping objects, the sequence of desired movements $x_{a,v}^d$ and $x_{b,v}^d$ should be calculated considering the distance between objects. Notice that the position of the j-th object $x_{a,j}^d$ is known in advance with the desired velocity $x_{b,j}^d = 0$. The information on the object's positions and the expected velocities governed the estimation of the reference trajectories.

State Constraints. The nature of the BR justifies that all the states (position and velocity) are uniformly bounded with respect to time; that is, the state $x^\top = [x_a^\top, x_b^\top]$ belongs to the state $X^+ = X_a^+ \cup X_b^+$, which is defined as:

$$\begin{aligned} X_a^+ &= \left\{ x_a \mid -\infty < x_{a,i}^- \leq x_{a,i} \leq x_{a,i}^+ < +\infty, \right\} \\ X_b^+ &= \left\{ x_b \mid -\infty < x_{b,i}^- \leq x_{b,i} \leq x_{b,i}^+ < +\infty, \right\} \end{aligned} \tag{6}$$

with x_i the i-th component of x, and the corresponding limits $\underset{t\geq 0}{sup}(x_i) + \epsilon = x_i^+$ and $\underset{t\geq 0}{inf}(x_i) - \epsilon = x_i^-$ with ϵ a small constant real scalar and x_i is either $x_{i,a}$ or $x_{i,b}$. The set X^+ defines the restrictions for the angular displacements and the angular velocities.

3.2. Description of the model for the robotic exoskeleton

The robotic exoskeleton includes three joints per lower limb, from where only two are actuated, leading to a total of four active joints. The mathematical description of the system is obtained through the Euler-Lagrange equations. The time-dependent model defines the dynamics of the generalized coordinates θ_1, and θ_2 as

$$\begin{aligned} \frac{d}{dt}\theta_1 &= \theta_2, \\ \frac{d}{dt}\theta_2 &= f(\theta_1, \theta_2) + g_a(\theta_1)u(t) + \xi(\theta_1, \theta_2, t), \end{aligned} \tag{7}$$

From here, $f : \mathcal{Z} \times \mathcal{Z} \to \mathbb{R}^n$, $\mathcal{Z} \subset \mathbb{R}^n$ defines the drifted dynamics associated to the robotic device, $g_a : \mathcal{Z} \to \mathbb{R}^{n\times n}$ characterizes the control associated dynamics, $\xi : \mathcal{Z} \times \mathcal{Z} \times \mathbb{R} \to \mathbb{R}^n$ represents the external perturbations and modeling errors effects on the manipulator dynamics, and $u_t \in \mathbb{R}^n$ corresponds to the control action effect on the device dynamics. The mechanical structure for the robotic arm implies that $\xi(\theta_1, \theta_2, t)$, considering the corresponding bounds for both perturbations and uncertainties, satisfies the next inclusion:

$$\|\xi(\theta_1, \theta_2, t)\| \leq \xi_0, \quad \xi_0 > 0. \tag{8}$$

From (8), notice that $\xi(\theta_1, \theta_2, t) \in \mathcal{L}_\infty^n$.

Considering the fundamentals of the Euler-Lagrange methodology, both functions f, and g_a are described as:

$$\begin{aligned} f(\theta_1, \theta_2) &= M^{-1}(\theta_1)(-C(\theta_1, \theta_2)\theta_2 - G(\theta_1)), \\ g_a(\theta_1) &= M^{-1}(\theta_1) \end{aligned} \tag{9}$$

In the expression (9), $C : \mathbb{R}^n \times \mathbb{R}^n \to \mathbb{R}^{n\times n}$ represents the matrix that related the Coriolis effects, $G : \mathbb{R}^n \to \mathbb{R}^n$ includes the effect of gravitational forces on the structure; and $M : \mathbb{R}^n \to \mathbb{R}^{n\times n}$ is the inertia matrix, which is assumed to be non-singular and invertible. The values for these elements are described in Appendix A. Taking into account the Euler-Lagrange basis, the condition $\|g_b(\theta_1)\|_\Gamma \leq g_b^0$, $g_b^0 > 0$ for all θ_1 and the corresponding positive matrix Γ, considering the application of the Frobenius norm.

The control scheme is based on the mathematical formulation of the system in (7). However, the control action $u(t)$ is defined based on hybrid position-force scheme, where the force control is activated when the force that is measured between the user and the device trespasses the reference force obtained from *Opensim* and shown in figure 4, and the position control is executed otherwise.

3.3. Position control of the lower limb exoskeleton

The first stage considers the trajectory tracking for each one of the active joints of the exoskeleton, considering as reference the trajectories obtained from *Opensim* throughout the gait cycle in healthy patients, as illustrated in figure 3. These trajectories are defined in terms of each joint's angular position during the gait cycle.

According to the mathematical description of the model in (7), the dynamic of the reference trajectory that is related to the angular position at each joint of the robotic exoskeleton can be represented as:

$$\begin{aligned} \frac{d}{dt}\theta_1^*(t) &= \theta_2^*(t), \\ \frac{d}{dt}\theta_2^*(t) &= h\big(\theta_1^*(t), \theta_2^*(t)\big). \end{aligned} \tag{10}$$

where $h : \mathcal{Z} \times \mathcal{Z} \to \mathbb{R}^n$ is the smooth vector field that describes the admissible reference trajectories.

The tracking force error for each joint of the device is defined based on the difference between the angular position and the reference $\delta = \theta^* - \theta$, where $\theta^* \in \mathbb{R}^{2n}$ and $\theta \in \mathbb{R}^{2n}$ with $\theta^* = \left[(\theta_1^*)^\top, (\theta_2^*)^\top\right]^\top$ and $\theta = \left[(\theta_1)^\top, (\theta_2)^\top\right]^\top$.

Taking into account both the equations from system (7) and the equations from (10), and based on the classical PID control algorithm, it is possible to define the control action $u(t) = u(\theta)$ for the trajectory tracking as:

$$\begin{aligned} u(\theta) = -g_a^{-1}[\theta_1(t)]\left(k_p\delta(t) + k_d\frac{d}{dt}\delta(t) + k_i\int\delta(t)\right) + \\ g_a^{-1}[\theta_1(t)]\left[h\left(\theta_1^*(t), \theta_2^*(t)\right) - f(\theta_1(t), \theta_2(t))\right] \end{aligned} \tag{11}$$

where k_p is the proportional gain, k_d is the derivative gain, and k_i is the integral gain. This controller is proposed as a reference framework to prove the hybrid position-force control scheme. Nonetheless, different controllers could be implemented to provide the systems with different capabilities, such as robustness.

3.4. Force control of the lower limb exoskeleton

The second stage of the proposed control algorithm is triggered when the measured force at each joint trespasses the reference force. Different from the position control section, this stage considers the inclusion of state constraints so that the force exerted over each joint remains bounded, avoiding any possible damage to the patient.
The mechanical structure of the robotic exoskeleton considers restrictions for the force F_ϵ that is generated between the user and the exoskeleton. Without loss of generality, in this study, asymmetric constraints are considered, with limitations that are represented as:

$$\Omega = \{F_\epsilon \mid -\infty < F_\epsilon^- < F_\epsilon < F_\epsilon^+ < +\infty\}, \tag{12}$$

Based on the definition of the restrictions for the coordinates in (12), the feasible positions for the exoskeleton end-effectors could be estimated considering the direct kinematics along with the corresponding Jacobian. Then, the control problem can be solved by considering the end-effector's motion, which can be related to the dynamic of the joints by applying the inverse kinematics of the device.

The proposed controller must then have the capability of forcing the system to track the reference trajectory and to stabilize the tracking error asymptotically to an invariant set that depends on the power of perturbations while considering the state restrictions from (12).

Considering the mathematical model of the system, there is a feasible set of references associated to the forces that are generated between the robotic device and the user represented as $F_\epsilon^* \in Z \subset \mathbb{R}^n$. The related states F_ϵ^* should satisfy:

$$\begin{aligned} \frac{d}{dt}F_{\epsilon,1}^*(t) = F_{\epsilon,2}^*(t), \\ \frac{d}{dt}F_{\epsilon,2}^*(t) = h\left(F_{\epsilon,1}^*(t), F_{\epsilon,2}^*(t)\right). \end{aligned} \tag{13}$$

Here $h : \mathcal{Z} \times \mathcal{Z} \to \mathbb{R}^n$ is a class of smooth vector field that defines the admissible reference trajectories.

The tracking force error for each joint of the device can be defined as $\sigma = F_\epsilon^* - F_\epsilon$, where $F_\epsilon^* \in \mathbb{R}^{2n}$ and $F_\epsilon \in \mathbb{R}^{2n}$ with $F_\epsilon^* = \left[(F_{\epsilon,1}^*)^\top, (F_{\epsilon,2}^*)^\top\right]^\top$ and $F_\epsilon = \left[(F_{\epsilon,1})^\top, (F_{\epsilon,2})^\top\right]^\top$.

Considering both the mathematical model and the dynamic of the reference trajectories, it is possible to define the control action $u(t) = u(F_\epsilon(t))$ that may solve the trajectory tracking issue as:

$$\begin{aligned} u(\theta(t), F_\epsilon(t)) = -g_a^{-1}[\theta_1(t)]K(t)\sigma(t) + \\ g_a^{-1}[\theta_1(t)]\left[h\left(F^*_{\epsilon,1}(t), F^*_{\epsilon,2}(t)\right) - f(\theta_1(t), \theta_2(t))\right] \end{aligned} \tag{14}$$

In (14), $K(t)$ defines the time-dependent control gain, where the state restrictions are considered as described in (12). This gain is used in the control action to enforce the system to track the desired trajectories while considering the class of aforementioned perturbations. The matrix A is selected as Hurwitz formed as

$$A = \begin{bmatrix} O_n & I_n \\ K_1^* & K_2^* \end{bmatrix} \tag{15}$$

The matrices $K_1^* \in \mathbb{R}^{n\times n}$ and $K_2^* \in \mathbb{R}^{n\times n}$ are selected to fulfil the Hurwitz nature of matrix A.

The temporal evolution of the variable gain $K(t)$ could be found as the solution for the differential equation given by:

$$2\gamma(t)\frac{d}{dt}K(t) + \left(\frac{d}{dt}\gamma(t) + \alpha\gamma(t)\right)\tilde{K}(t) + \sigma(t)\sigma^\top(t)PB = 0. \tag{16}$$

where σ^+ defines the upper bound of the norm of σ, that is $\|\sigma\|^2 < \sigma^+$, $\tilde{K}(t) = K(t) - K^*$, with $K^* = [K_1^*, K_2^*]$ that must be selected according to the following rule: $A - BK^*$ is a Hurwitz matrix with $B = [0_n, I_n]^\top$. The inclusion of $\epsilon > 0$ allows the inclusion of the invariant characteristic of the set where the tracking error converges.

The expression that defines the adaptive gain $K(t)$ can be derived from (16), yielding:

$$K(t) = \int_{\tau=0}^{t} \frac{-(\dot{\gamma} + \alpha\gamma)\tilde{K}(t) - \sigma(t)\sigma^\top(t)PB}{2\gamma} d\tau \tag{17}$$

The controller form is illustrated using all the components considering motion restrictions and the laws describing the evolution of the adaptive gains.
The constraints defined in (12) are included in the term $\gamma(t)$, which is selected as positive and varies depending on the admissible states within the constraint set. The evolution of $\gamma(t)$ is defined as follows:

$$\gamma(t) = \left(\frac{F^+_{\epsilon,1} - F_{\epsilon,1}(t)}{F^+_{\epsilon,1}} \times \frac{F^-_{\epsilon,1} - F_{\epsilon,1}(t)}{F^-_{\epsilon,1}}\right) \tag{18}$$

Figure 8 shows the general diagram of the control approach, where both the position and force controller are described. Notice that the control selector section chooses which controller to use based on whether the measured force trespasses the reference force or not.

4. Aspects of the control implementation

5. Simulated Results

A novel strategy of

6. Discussion

7. Conclusions

Author Contributions: "Conceptualization, X.X. and Y.Y.; methodology, X.X.; software, X.X.; validation, X.X., Y.Y. and Z.Z.; formal analysis, X.X.; investigation, X.X.; resources, X.X.; data curation,

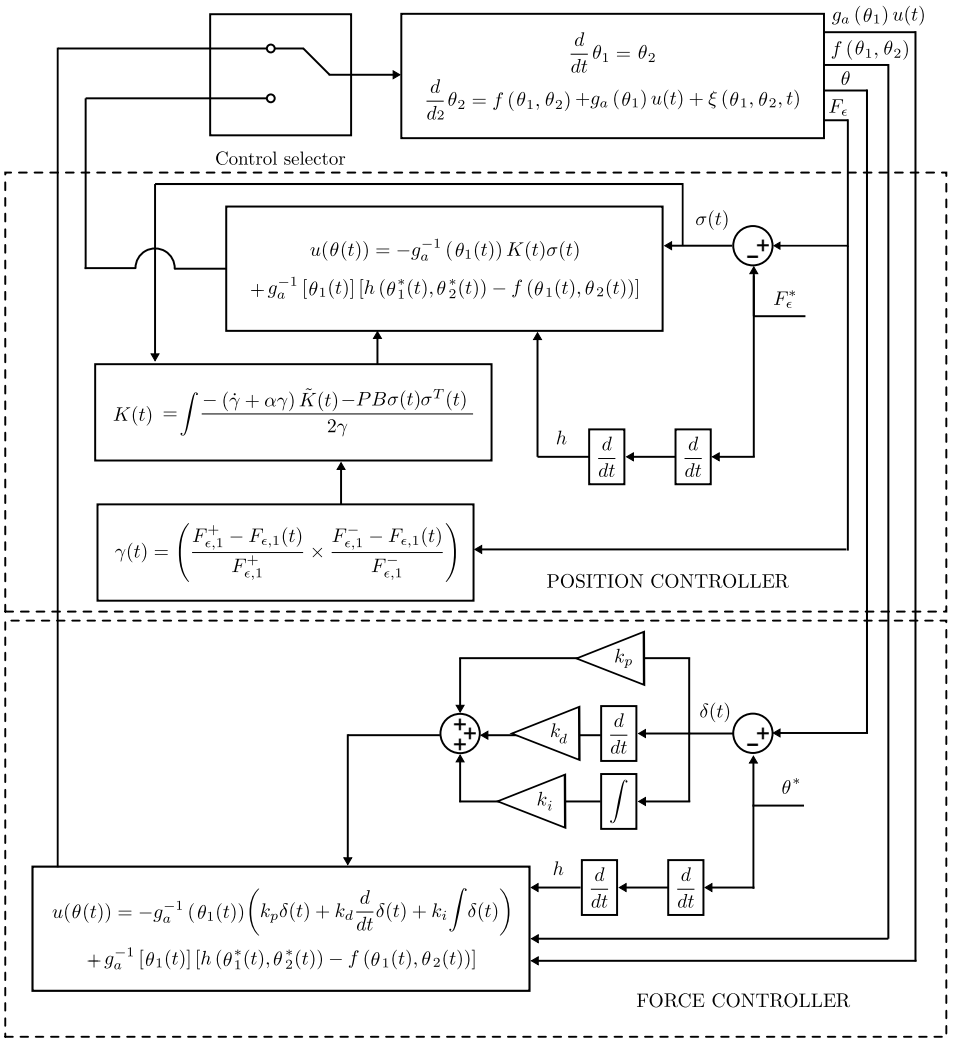

Figure 8. Hybrid position force control diagram

X.X.; writing—original draft preparation, X.X.; writing—review and editing, X.X.; visualization, X.X.; supervision, X.X.; project administration, X.X.; funding acquisition, Y.Y. All authors have read and agreed to the published version of the manuscript."

Funding: This research was funded by Consejo Nacional de Ciencia y Tecnología (CONACYT) and Tecnologico de Monterrey, Institute of Advanced Materials for Sustainable Manufacturing under the grant Challenge-Based Research Funding Program 2022 number I006-IAMSM004-C4-T2-T.

Data Availability Statement: The data presented in this study are available on request from the corresponding author.

Conflicts of Interest: The authors declare no conflict of interest.

Appendix A Mathematical model based on Euler-Lagrange Equations

According to the conventional representation of second order mechanical systems based on Euler-Lagrange formulation, the following equation describes the dynamic of the system:

$$M(\theta)\ddot{\theta} + C(\theta, \dot{\theta})\dot{\theta} + G(\theta) = \tau \tag{A1}$$

which is represented in its matrix form as:

$$\begin{bmatrix} M_{11} & M_{12} \\ M_{21} & M_{22} \end{bmatrix} \begin{bmatrix} \ddot{\theta}_1 \\ \ddot{\theta}_2 \end{bmatrix} + \begin{bmatrix} C_{11} & C_{12} \\ C_{21} & C_{22} \end{bmatrix} \begin{bmatrix} \dot{\theta}_1 \\ \dot{\theta}_2 \end{bmatrix} + \begin{bmatrix} G_1 \\ G_2 \end{bmatrix} = \begin{bmatrix} \tau_1 \\ \tau_2 \end{bmatrix} \tag{A2}$$

where

$$M_{11} = \frac{1}{4}\left[m_1 l_1^2 + m_2(4l_1^2 + l_2^2)\right] + m_2 l_1 l_2 cos(\theta_2) \tag{A3}$$

$$M_{12} = -\left[\frac{1}{4} m_2 l_2^2 + \frac{1}{2} m_2 l_1 l_2 cos(\theta_2)\right] \tag{A4}$$

$$M_{21} = -\left[\frac{1}{4} m_2 l_2^2 + \frac{1}{2} m_2 l_1 l_2 cos(\theta_2)\right] \tag{A5}$$

$$M_{22} = \frac{1}{4} m_2 l_2^2 \tag{A6}$$

$$C_{11} = \left(m_1 g \frac{l_1}{2} + m_2 g l_1\right) sin(\theta_1) + \left(m_2 g \frac{l_1}{2}\right) sin(\theta_1 - \theta_2) \tag{A7}$$

$$C_{12} = \frac{1}{2} m_2 l_1 l_2 \dot{\theta}_2 sin(\theta_2) - m_2 l_1 l_2 \dot{\theta}_1 sin(\theta_2) \tag{A8}$$

$$C_{21} = \frac{1}{2} m_2 l_1 l_2 \dot{\theta}_1 sin(\theta_2) \tag{A9}$$

$$C_{22} = m_2 l_1 l_2 \dot{\theta}_1 sin(\theta_2) \tag{A10}$$

$$G_1 = 0 \tag{A11}$$

$$G_2 = -\left(m_2 g \frac{l_2}{2}\right) sin(\theta_1 - \theta_2) \tag{A12}$$

References

1. Dollar, A.M.; Herr, H. Lower extremity exoskeletons and active orthoses: Challenges and state-of-the-art. *IEEE Trans. Robot.* **2008**, *24*, 144–158.
2. Lee, H.; Ferguson, P.W.; Rosen, J. Lower limb exoskeleton systems—overview. In *Wearable Robotics*; Elsevier, 2020; pp. 207–229.
3. Baud, R.; Manzoori, A.R.; Ijspeert, A.; Bouri, M. Review of control strategies for lower-limb exoskeletons to assist gait. *J. Neuroeng. Rehabil.* **2021**, *18*, 119.
4. Shi, D.; Zhang, W.; Zhang, W.; Ding, X. A review on lower limb rehabilitation exoskeleton robots. *Chin. J. Mech. Eng.* **2019**, *32*.
5. Raibert, M.H.; Craig, J.J. Hybrid position/force control of manipulators **1981**.
6. Henderson, H. *Modern robotics: building versatile machines*; Infobase Publishing, 2006.
7. Mueller, A. Modern robotics: Mechanics, planning, and control [bookshelf]. *IEEE Control Systems Magazine* **2019**, *39*, 100–102.
8. Pérez-San Lázaro, R.; Salgado, I.; Chairez, I. Adaptive sliding-mode controller of a lower limb mobile exoskeleton for active rehabilitation. *ISA Trans.* **2021**, *109*, 218–228.
9. Delp, S.L.; Anderson, F.C.; Arnold, A.S.; Loan, P.; Habib, A.; John, C.T.; Guendelman, E.; Thelen, D.G. OpenSim: open-source software to create and analyze dynamic simulations of movement. *IEEE Trans. Biomed. Eng.* **2007**, *54*, 1940–1950.
10. Xu, X.; McGorry, R.W.; Chou, L.S.; Lin, J.H.; Chang, C.C. Accuracy of the Microsoft Kinect for measuring gait parameters during treadmill walking. *Gait Posture* **2015**, *42*, 145–151.
11. Hurmuzlu, Y.; Génot, F.; Brogliato, B. Modeling, stability and control of biped robots—a general framework. *Automatica* **2004**, *40*, 1647 – 1664. https://doi.org/10.1016/j.automatica.2004.01.031.

12. Sinnet, R.W.; Powell, M.J.; Shah, R.P.; Ames, A.D. A Human-Inspired Hybrid Control Approach to Bipedal Robotic Walking. *IFAC Proceedings Volumes* **2011**, *44*, 6904 – 6911. 18th IFAC World Congress, https://doi.org/10.3182/20110828-6-IT-1002.03802.
13. Cruz, D.; Luviano-Juárez, A.; Chairez, I. Output sliding mode controller to regulate the gait of Gecko-inspired robot. In Proceedings of the Memorias del XVI Congreso Latinoamericano de Control Automático, CLCA 2014; , 2014.
14. Grizzle, J.W.; Chevallereau, C.; Sinnet, R.W.; Ames, A.D. Models, feedback control, and open problems of 3D bipedal robotic walking. *Automatica* **2014**, *50*, 1955 – 1988. https://doi.org/10.1016/j.automatica.2014.04.021.
15. Hargraves, C.R.; Paris, S.W. Direct trajectory optimization using nonlinear programming and collocation. *Journal of Guidance, Control, and Dynamics* **1987**, *10*, 338–342. https://doi.org/10.2514/3.20223.
16. Merchant, R.; Cruz-Ortiz, D.; Ballesteros-Escamilla, M.; Chairez, I. Integrated wearable and self-carrying active upper limb orthosis. *Proceedings of the Institution of Mechanical Engineers, Part H: Journal of Engineering in Medicine* **2018**, *232*, 172–184.
17. Gaytán, A.; Sanchez-Magos, M.; Cruz-Ortiz, D.; Ballesteros-Escamilla, M.; Salgado, I.; Chairez, I. Adaptive Proportional Derivative Controller of Cooperative Manipulators. *IFAC-PapersOnLine* **2018**, *51*, 232–237.